Anal Bioanal Chem
DOI 10.1007/s00216-016-9358-6

RESEARCH PAPER

Label-free and sensitive aptasensor based on dendritic gold nanostructures on functionalized SBA-15 for determination of chloramphenicol

Ayemeh Bagheri Hashkavayi[1] · Jahan Bakhsh Raoof[1] · Razieh Azimi[1] · Reza Ojani[1]

Received: 2 November 2015 / Revised: 16 January 2016 / Accepted: 22 January 2016

Abstract A highly sensitive and low-cost electrochemical aptasensor was developed for the determination of chloramphenicol (CAP). The system was based on a CAP-binding aptamer, a molecular recognition element, and 1,4-diazabicyclo[2.2.2]octane (DABCO)-supported mesoporous silica SBA-15 on the surface of a screen-printed graphite electrode for formation of dendritic gold nanostructures and improving the performance and conductivity of the biosensor. Hemin has been applied as an electrochemical indicator which interacted with the guanine bases of the aptamer. In the absence of CAP, hemin binds to the aptamer and produces a weak differential pulse voltammetric (DPV) signal. The presence of CAP led to stabilization of the folded aptamer, which generated an amplified DPV signal. The peak current of hemin increased linearly with the concentration of CAP. Under optimal conditions, two linear ranges were obtained from 0.03 to 0.15 μM and 0.15 to 7.0 μM, respectively, and the detection limit was 4.0 nM. The prepared biosensor has good selectivity against other non-target drugs. Thus, the sensor could provide a promising platform for the fabrication of aptasensors. The feasibility of using this aptasensor was demonstrated by determination of CAP in a human blood serum sample.

Keywords Aptamer · Chloramphenicol · SBA-15@DABCO · Hemin · Dendritic gold nanostructures · Screen-printed graphite electrode

Introduction

Aptamers are single-stranded oligonucleic acids or peptide molecules, which can be obtained by an in vitro selection process called systematic evolution of ligands by exponential enrichment (SELEX) [1, 2]. Owing to their three-dimensional structure (3D), aptamers can specifically bind to a variety of targets, such as enzymes, antibodies, and drugs [3]. A variety of aptasensors have been developed using different analytical methods. For example, surface plasmon resonance spectroscopy [4], microgravimetry [5], quartz crystal microbalance [6], fluorescence [7], and electrochemistry [8]. Electrochemical aptasensors have received much attention owing to their distinct advantages, such as simplicity, low cost, rapid response, and high sensitivity and stability [9, 10]. The performance of aptasensors can be significantly improved by amplifying the electrochemical signals using different nanomaterials, such as silica nanoparticles [11], magnetic beads [12], organic polymers [13], and silver nanoparticles [14]. One of these materials is mesoporous silica SBA-15. SBA-15 is a promising candidate for the immobilization of various materials and can be used to create stable biosensing systems owing to its high surface to area ratio, porosity, uniform pore size distributions, and thermal stability [15]. In this article, the synthesized SBA-15 was functionalized using 1,4-diazabicyclo[2.2.2]octane (DABCO) and produced an ionic liquid framework on the surface of SBA-15. Gold nanoparticles (AuNPs) were then electrochemically deposited on the SBA-15@DABCO surface. Ionic liquids (ILs) have been used as electrolytes and potent solvents [16]. ILs have

Electronic supplementary material The online version of this article (doi:10.1007/s00216-016-9358-6) contains supplementary material, which is available to authorized users.

✉ Jahan Bakhsh Raoof
j.raoof@umz.ac.ir

[1] Electroanalytical Chemistry Research Laboratory, Department of Analytical Chemistry, Faculty of Chemistry, University of Mazandaran, Babolsar, Mazandaran 47416-1467, Iran

Published online: 15 February 2016

remarkable properties, such as very low vapor pressure, large working temperature range (−40 to +200 °C), high mechanical stability, high electrochemical stability, low toxicity, and inexpensive production, that make them favorable candidates for producing electrochemical aptasensors [17, 18].

In addition to the aforementioned advantages of ionic liquid frameworks, the N groups on SBA-15@DABCO could also help the deposition of more Au nanoparticles and formation of dendritic Au nanostructure on SBA-15@DABCO and prevent the aggregation of Au nanoparticles.

Hemin (HEM) is a porphyrin which has four pyrrole moieties. The pyrroles are cyclically connected to each other, and an Fe(III) ion is located in the center of the structure [19]. HEM is an electrochemical indicator that is reduced at carbon surfaces at a potential of around −0.37 V vs. Ag/AgCl electrode [20]. The reduction process includes transferring an electron from the negatively charged electrode to the positively charged HEM. HEM, which is an electrochemical indicator, could also interact with nucleic acids [21]. Chloramphenicol (CAP) {2,2-dichloro-*N*-[2-hydroxy-1-(hydroxymethyl)-2-(4-nitrophenyl)ethyl]acetamide}, is a broad-spectrum antibiotic that was first produced by the soil bacterium *Streptomyces venezuelae* [22] and is used for the treatment of infectious diseases in animals and humans. This antibiotic has several side effects such as aplastic anemia and genotoxicity in humans. Thus, the European Union (EU) has set a maximum residue limit (MRL) standard for CAP in foodstuffs of animal origin at a level of 0.3×10^{-6} g kg^{-1} [23]. Several analytical methods have been reported for the determination of CAP in various samples, such as liquid chromatography (LC) [24], capillary zone electrophoresis [25], liquid chromatography– electrospray ionization tandem mass spectrometry (LC-ESI–MS/MS) [26], planar chromatography [27], gas chromatography–mass spectrometry (GC–MS) [28], chemiluminescence [29], and spectrophotometry [30]. Although these methods could be used to detect CAP, they are expensive, tedious, and operationally complex; hence, the development of a highly sensitive and selective aptasensor for the detection of CAP is very important. The present study describes a sensitive electrochemical method for the detection of CAP in which the molecular recognition element is an aptamer. HEM also interacts with guanine bases of the aptamers and acts as an electrochemical indicator. Controlling the immobilization of the aptamer on the electrode surface is an important step in designing this electrochemical aptasensor. For this purpose, a carbon screen-printed electrode (SPE) was modified with the SBA-15@DABCO. The electrodeposition of the AuNPs was performed to transfer these particles onto the SBA-15 functionalized surface and lead to the formation of dendritic gold nanostructures. This step connects the thiolated aptamer on the electrode by Au–S bonds. The constructed dendritic AuNPs/SBA-15@DABCO has a large specific surface area, good biocompatibility, and high conductivity.

Experimental

Chemicals and reagents

The DNA aptamer with 5'-thiol modification was purified with HPLC (MWG-BIOTECH, Germany). The sequence of the aptamer was as follows [31]:

5'-(SH)-$(CH_2)_6$-AGCAGCACAGAGGTCAG ATGACTTCAGTGAGTTGTCCCACGGTCGGCGA-GTCGG TGGTAGCCTATGCGTGCTACCGTGAA-3'

Healthy human serum sample for real sample analysis was supplied by the North Research Center, Pasteur Institute of Iran (Amol, Iran) with ethical approval. All reagents were of analytical grade and purchased from Aldrich or Merck. Doubly deionized water was used for the preparation of working solutions. The stock solution of aptamer (2.0 μM) was prepared from Tris–HCl buffer (20 mM Tris–HCl, 0.1 M NaCl, 0.2 M KCl, 5 mM $MgCl_2$, pH 7.4) and the solution was kept frozen.

Apparatus

Graphite SPEs (purchased from Florence, Italy) consisted of a carbon working electrode (3 mm in diameter), silver pseudoreference electrode, and carbon counter electrode. Materials and procedures used to screen print the transducers were described elsewhere [32].

An Autolab PGstut 30 electrochemical analysis system controlled by GPES 4.9 and FRA software (Eco Chemie Netherlands) was used in electrochemical studies. Scanning electron microscopy images were obtained using a Mira 3-XMU Field Emission SEM (FESEM) system. FT-IR spectra were obtained on a Shimadzu instrument. TGA was recorded on a Stanton Redcraft STA-780 (London, UK). Elemental analyses were carried out with a Perkin Elmer CHN 2400 instrument. Transmission electron microscopy (TEM) images were observed under a TEM-PHILIPS-CM10HT100KV instrument. Melting points were determined on a Thermo Scientific IA9200 and XRD patterns of the synthesized SBA-15@DABCO were recorded by an X-ray

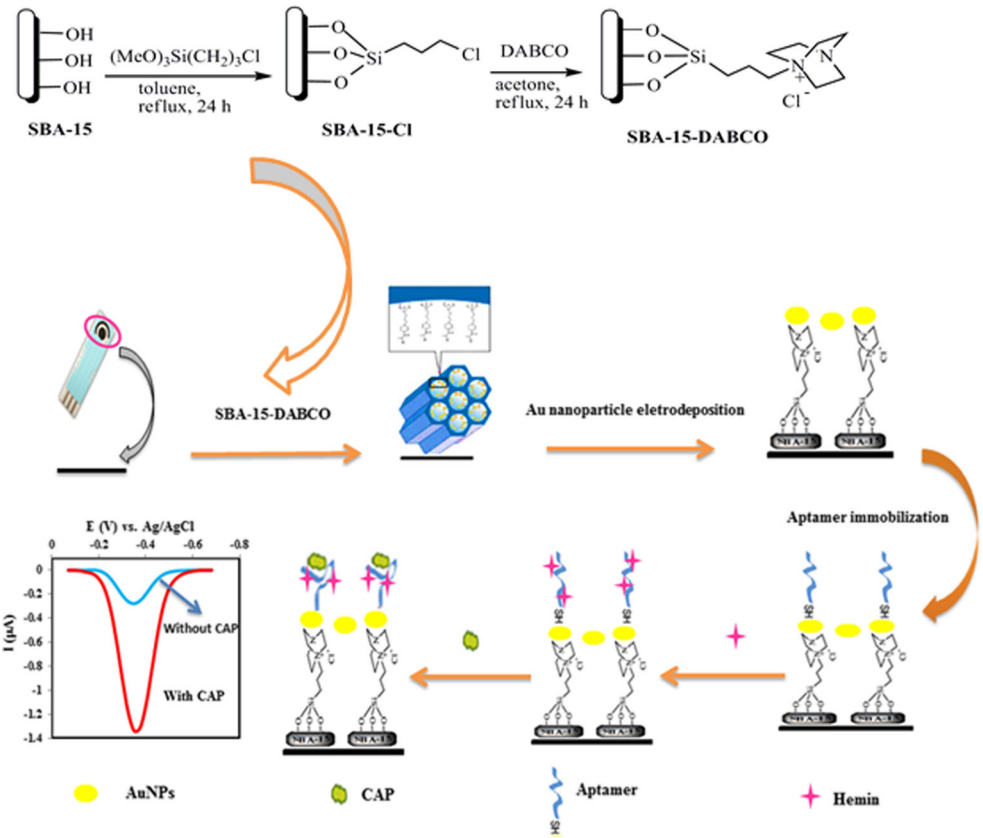

Scheme 1 Synthesis of SBA-15@DABCO and schematic representation of the preparation of aptasensor for detection of CAP

diffractometer (XRD, GBC MMA Instrument) with Be-filtered Cu Kα radiation.

Procedure

Preparation of SBA-15@DABCO

The SBA-15@DABCO was synthesized by a typical heterogeneous process that is shown in Scheme 1. The SBA-15 was prepared according to the literature procedure [33].

First, the SBA-15 (1 g) was dispersed in boiling toluene (25 mL). Then, the (3-chloropropyl)trimethoxysilane (1.5 mL) was added dropwise and the mixture was refluxed for 24 h. The resultant solid was filtered and extracted in a continuous extraction (Soxhlet) apparatus in the presence of dichloromethane. Then, this mixture was dried under vacuum at 70 °C for 5 h to form the SBA-15@Cl.

The SBA-15@Cl (1 g) was refluxed with DABCO (73 mg) in acetone (60 mL) for 24 h under argon atmosphere. The product was filtered and extracted with dichloromethane in a Soxhlet extractor overnight. The resulting material was dried under vacuum for 4 h at 50 °C to generate the SBA-15@DABCO.

Preparation of modified graphite screen-printed electrode

A 7-μL droplet of SBA-15@DABCO was dropped on the working electrode surface. Then, this droplet was dried at room temperature for 2.0 h. Next, it was rinsed with ultrapure water to remove the unabsorbed SBA-15@DABCO. The electrodeposition of AuNPs was carried out by chronoamperometry at −0.23 V for 300 s using a solution containing 0.5 mM $HAuCl_4$ to form dendritic gold nanostructures on the surface of SBA-15@DABCO/SPE.

Immobilization of aptamer onto AuNPs/SBA-15@DABCO/SPE surface and interaction with CAP

The interaction of the aptamer with CAP on the modified SPE surface was investigated in three steps: First, 7 μL of 2 μM aptamer solution was placed on the modified SPE and this solution was incubated for 7 h at room temperature. Then, 7 μL of 20 μM HEM solution was added to the modified SPE for 15 min. Subsequently, 7 μL of CAP solution with different concentrations was dropped on the immobilized Apt/AuNPs/SBA-15@DABCO/SPE for 30 min. The electrode was rinsed with deionized water after each incubation step.

The fabrication process for the CAP aptasensor is shown in Scheme 1. The differential pulse voltammetric data were

obtained in 50 mM Tris–HCl buffer solution (TBS) and in the range of −0.07 and −0.7 vs. Ag/AgCl/KCl (3 mol L^{-1}) at a scan rate of 50 mV s^{-1} with an amplitude of 50 mV and pulse width of 0.05 s.

Results and discussion

Analysis of SBA-15@DABCO

Figure 1A shows the FT-IR spectra of the SBA-15, SBA-15@Cl, and SBA-15@DABCO. The peaks around 465, 800, and 1100 cm^{-1} are for the Si–O–Si band which is ascribed to the presence of the condensed silica network in SBA-15 materials [34]. The absorption bands at 1630 and 3450 cm^{-1} are most probably due to the O–H vibration of silanol groups and physisorbed water for all samples [35]. The band at 960 cm^{-1} (Fig. 1A, curve a) is assigned to Si–O stretching of the surface silanols [34, 36]. The characteristic peaks at about 2800 and 1460 cm^{-1} are attributed to the C–H stretching and CH_2 bending of the propyl spacer and cycloalkane ring, respectively (Fig. 1A, curves b, c). Moreover, the peak at 1615 cm^{-1}, which is characteristic for the C–N^+ stretching, implied that DABCO had been loaded onto the support (Fig. 1A, curve c) [37].

The quantity of the DABCO attached on the mesoporous silica SBA-15 was calculated by the nitrogen content, 0.82 mmol/g, based on the elemental analysis (C: 9.26 %; H: 1.07 %; N: 2.32 %). The loading level of DABCO based on the chlorine content was similar (0.83 mmol/g). Further investigations by potentiometric titration [38] were in line with the elemental analysis and TGA results.

XRD measurements of the SBA-15@DABCO (Fig. 1B) showed three peaks, a single intense reflection at 2θ angle around 0.8° and two weak peaks around 2θ = 1.5° and 1.7°, which are assigned to 100, 110, and 200 reflections of the highly ordered arrangement of two dimensional hexagonal channels [33, 34]. The thermal stability of the SBA-15 and SBA-15@DBCO was investigated by thermogravimetry (TG) analysis. The profiles show that the SBA-15 silica material had a relatively high level of thermal stability and the 1.32 % weight loss below 150 °C in the thermogram of SBA-15@DABCO might be due to the adsorbed water on the surface of the catalyst [39]. In the temperature range of 220–

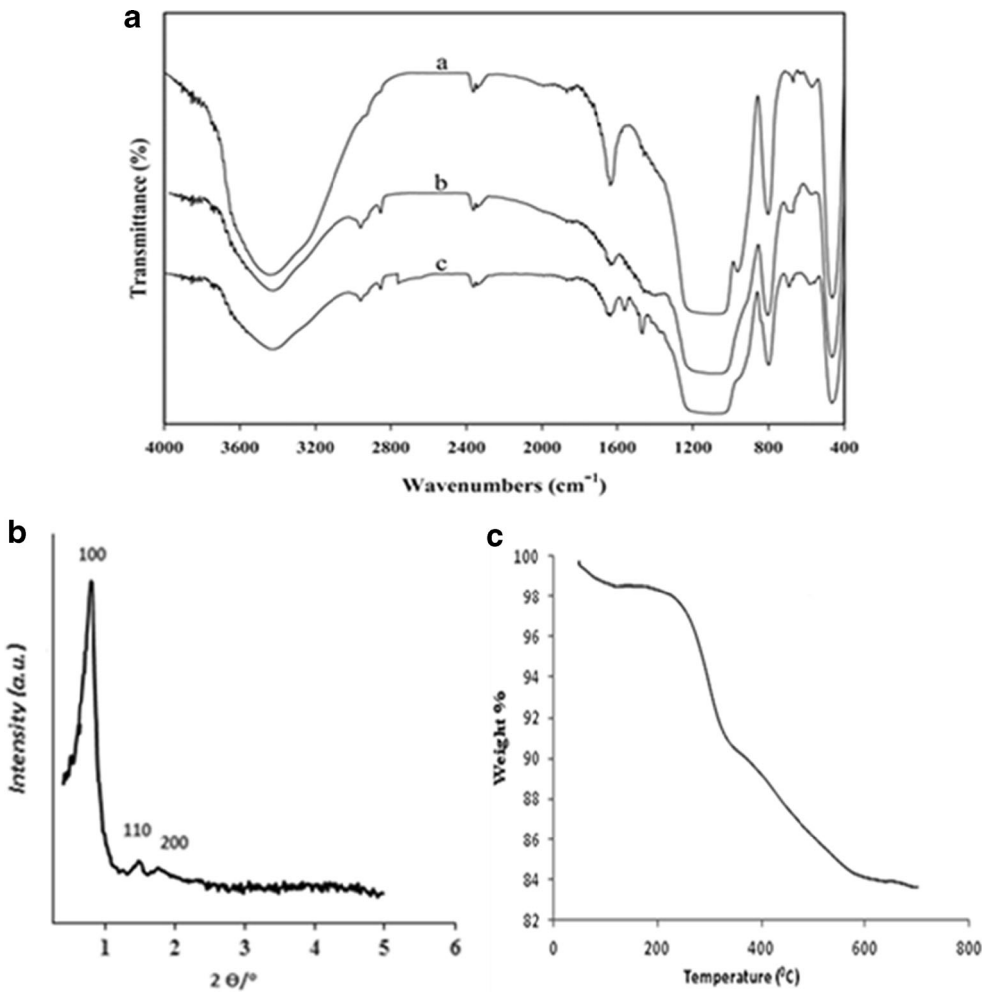

Fig 1 (**A**) FT-IR spectra of (a) SBA-15, (b) SBA-15@Cl, and (c) SBA-15@DABCO. (**B**) XRD pattern and (**C**) TGA curve of SBA-15@DABCO

600 °C, a complete loss of the organic species was observed (Fig. 1C).

Electrode modification

Figure 2A illustrates TEM images of SBA-15@DABCO. TEM study established the 2D mesostructure of the SBA-15 material and hexagonal pore arrays [33, 40]. The average pore diameter of the SBA-15@DABCO estimated by the TEM measurements was ca. 6 nm.

SEM images of the modified SPEs are shown in Fig. 2B, C. Figure 2B shows the mesoporous structure for the SBA-15@DABCO/SPE with nano-sized parallel channels. Figure 2C shows the morphology of the dendritic AuNPs/SBA-15@DABCO/SPE. The AuNPs were deposited on the SBA-15@DABCO channels. The amine groups on the DABCO can enhance the AuNPs deposition in the SBA-15@DABCO channels through the formation of N–Au bonds.

Electrochemical characterization of modified electrode

The changes in the characteristics of the surface of SPE modifications could be monitored using cyclic voltammetry (CV) and electrical impedance spectroscopy (EIS) techniques. Cyclic voltammetric responses of 0.01 M $[Fe(CN)_6]^{3-/4-}$ and 100 mM KCl at a scan rate of 100 mV s^{-1} on the bare SPE, SBA-15@DABCO/SPE, AuNPs/SBA-15@DABCO/SPE, and Apt/AuNPs/SBA-15@DABCO/SPE are shown in Fig. 3A. Curve a shows that a couple of well-defined redox peaks could be observed at the bare SPE. The ΔE_p value of the surface of bare SPE was about 722 mV, which indicates that the electron transfer kinetics were limited. After electrode modification with the SBA-15@DABCO, the porous structure of SBA-15@DABCO leads to an increase in current response of $[Fe(CN)_6]^{3-/4-}$ (curve b) compared to that of bare electrode (curve a). After the AuNPs electrodeposition on the SBA-15@DABCO/SPE, the intensity of the $[Fe(CN)_6]^{3-/4-}$ signal notably increased with a decrease in ΔE_p (curve c), which can be attributed to the large electron transfer ability and high specific surface area of AuNPs. Upon the immobilization of the aptamer on the dendritic AuNPs/SBA-15@DABCO, the current response decreased and ΔE_p became 259 mV. This phenomenon is due to the repulsive electrostatic interactions between the negative phosphate backbone of the aptamer and the $[Fe(CN)_6]^{3-/4-}$ anions indicating that most of the electrode surface is covered by the aptamer

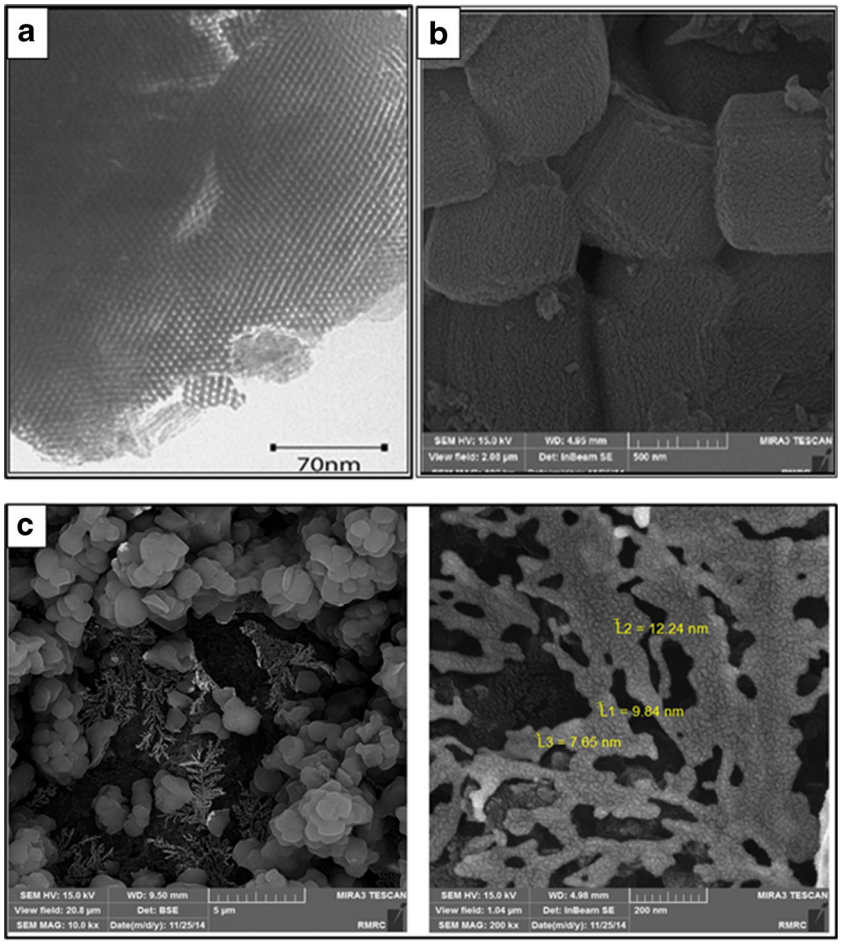

Fig. 2 (**A**) TEM image of SBA-15@DABCO, (**B**) and (**C**) SEM images of SBA-15@DABCO, AuNPs/SBA-15@DABCO/SPE

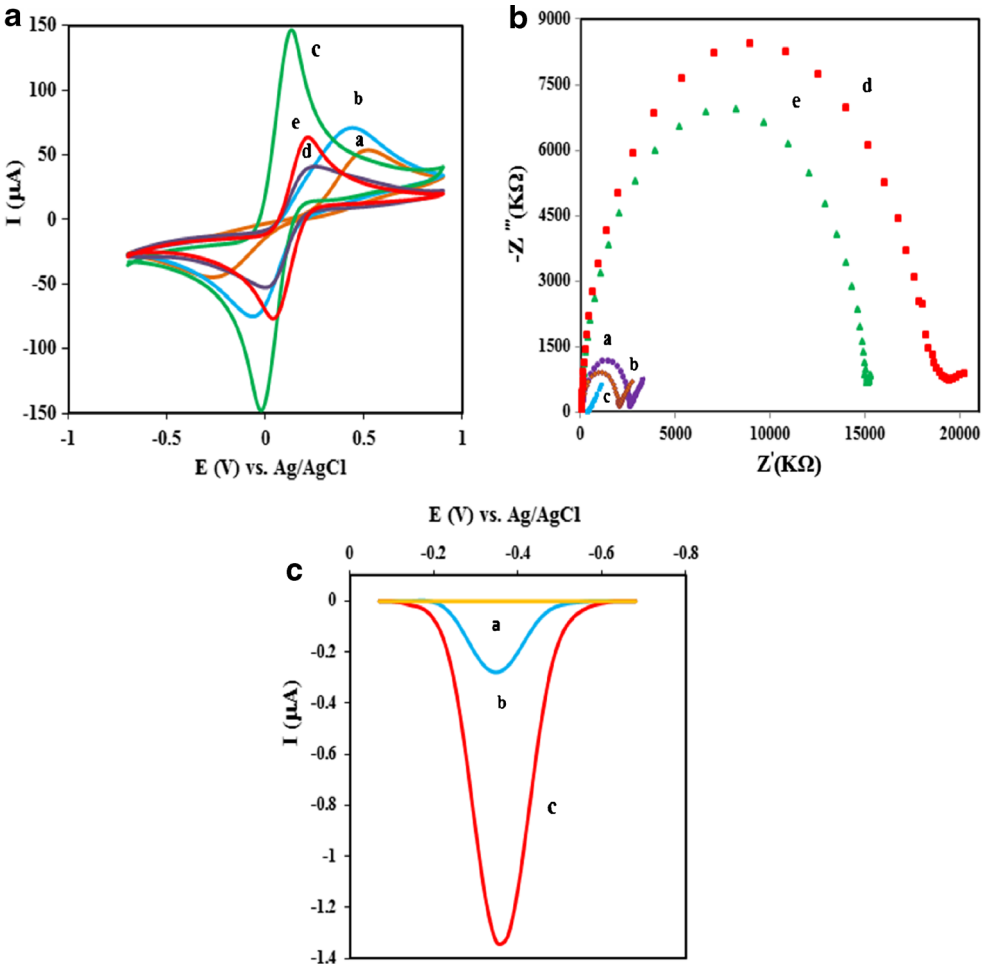

Fig. 3 (**A**) Cyclic voltammograms and (**B**) Nyquist plots of impedance spectra of different modification steps of aptasensor: (a) bare SPE, (b) SBA-15@DABCO/SPE, (c) AuNPs/SBA-15@DABCO/SPE, (d) Apt/AuNPs/SBA-15@DABCO/SPE, and (e) CAP/Apt/AuNPs/SBA-15@DABCO/SPE in 50 mM Tris–HCl buffer solutions (pH 7.40) containing 0.01 M $K_3[Fe(CN)_6]$/$K_4[Fe(CN)_6]$ (1:1) and 100 mM KCl. (**C**) DPV signals of (a) HEM/SBA-15@DABCO/SPE, (b) HEM/Apt/AuNPs/SBA-15@DABCO/SPE, and (c) HEM/Apt/AuNPs/SBA-15@DABCO/SPE after incubation for 30 min with 6.0 μM CAP, in 50 mM Tris–HCl buffer solution (pH 7.40)

(curve d). Upon binding of CAP to the aptamer-modified electrode, the peak current increased distinctly (curve e). This was ascribed to the fact that the formation of Apt–CAP complex induces folding and conformational change in the aptamer structure.

To further investigate the generation of the desired aptasensor, we used EIS to generate the Nyquist plots of the faradic impedance spectra at the different electrodes in 50 mM TBS (pH 7.40) containing 0.01 M $[Fe(CN)_6]^{3-/4-}$ (1:1) and 100 mM KCl (Fig. 3B). Nyquist plots include a semicircle portion at higher frequencies corresponding to the electron-transfer-limited process and a linear part at the lower frequency range corresponding to the diffusion-limited process. To analyze the surface properties during the fabrication of the aptasensor, the change in the values of R_{ct} for different steps was elected. First, the EIS of the bare SPE exhibited a very small semicircle and its R_{ct} is 2500 Ω (curve a). It can be seen that for SBA-15@DABCO/SPE, the value of R_{ct} decreased compared to the bare SPE as a result of the low resistance of SBA-15@DABCO in the redox couple (curve b). After the SBA-15@DABCO/SPE was coated with AuNPs, the value of R_{ct} decreased compared to the SBA-15@DABCO/SPE, which indicates a higher electron transfer capability and electronic conductivity of the immobilized AuNPs at the SBA-15@DABCO/SPE (curve c). When the thiol-terminated aptamer was self-assembled onto dendritic AuNPs/SBA-15@DABCO/SPE for 7 h, the R_{ct} increased to 18,470 Ω (curve d). This increase can be ascribed to an electrostatic repulsive force between the negative charges on the phosphate backbone of the self-assembled monolayer (SAM) aptamer and the negatively charged probe $[Fe(CN)_6]^{3-/4-}$ anions. Incubation of the Apt/AuNPs/SBA-15@DABCO/SPE with 2 μM CAP for 30 min led to a decrease in the R_{ct} value up to 15,000 Ω (curve e). This is attributed to the interaction of aptamer with CAP and deformation of the aptamer. This change made the reception of the $[Fe(CN)_6]^{3-/4-}$ at the aptasensor surface occur more freely. The above results indicated the successful construction of the aptasensor.

Optimization of experimental conditions

The experimental parameters such as aptamer concentration, aptamer immobilization time, incubation time, and pH were optimized for the analysis of the CAP.

The effect of the self-assembly time on the current response of the aptasensor was investigated between 2.0 and 9.0 h. Figure S1A in the Electronic Supplementary Material (ESM) demonstrates that the DPV response was increased by increasing the self-assembly time from 2.0 h to 9.0 h. However, after 7.0 h the response was constant. Therefore, the optimal time was chosen as 7.0 h.

The effects of aptamer concentrations on the signal of HEM reduction were studied by applying different concentrations (0.5–3.5 μM) of aptamer to the dendritic AuNPs/SBA-15@DABCO (ESM Fig. S1B). After incubating for 7.0 h, 7 μL of 20 μM HEM solution was added to the modified SPE for 15 min. Then, the modified electrode was treated with 7 μL of 2 μM CAP in 50 mM TBS (pH 7.2) for 30 min. The electrode was rinsed with deionized water after each incubation step and DPVs were recorded for different concentrations of aptamer-modified sensors. The current response increased with increasing aptamer concentrations. When it reached to 2.0 μM, there was no significant increase in the response of aptasensor. In addition, the current had reached a steady state due to the saturation of the active sites for immobilizing the aptamer. Therefore, the concentration of 2.0 μM was selected as an optimized aptamer concentration in this experiment.

The effect of the incubation time of the interaction between CAP and the thiolated aptamer on the current response of the aptasensor was also investigated. The current response of the aptasensor increased with longer reaction times from 0 to 30 min and reached a plateau at 30 min. This result implies that the formation of the aptamer–CAP complexes was completed after 30 min. Thus, a 30-min incubation time was used in these experiments (ESM Fig. S1C). The effect of pH on CAP detection was studied by recording the DPV over a range of 4.0–8.3 in 50 mM of TBS (ESM Fig. S1D). The reduction current increased as the pH increased from pH 4.0 to 7.4 and reached a steady state at pH 7.4. Thus, pH 7.4 was the optimum pH to achieve a high sensitivity.

Electrochemical investigation of interaction of aptamer with CAP

In this work, DPV was employed to establish several steps for the preparation of the aptasensor (Fig. 3C). Significant changes in the DPV signal took place in the area of the HEM reduction (−0.07 to −0.7 V). Curve a in Fig. 3C shows the DPV signal for the AuNPs/SBA-15@DABCO in 50 mM TBS (pH 7.4) in the presence of 20 μM HEM. Upon addition of

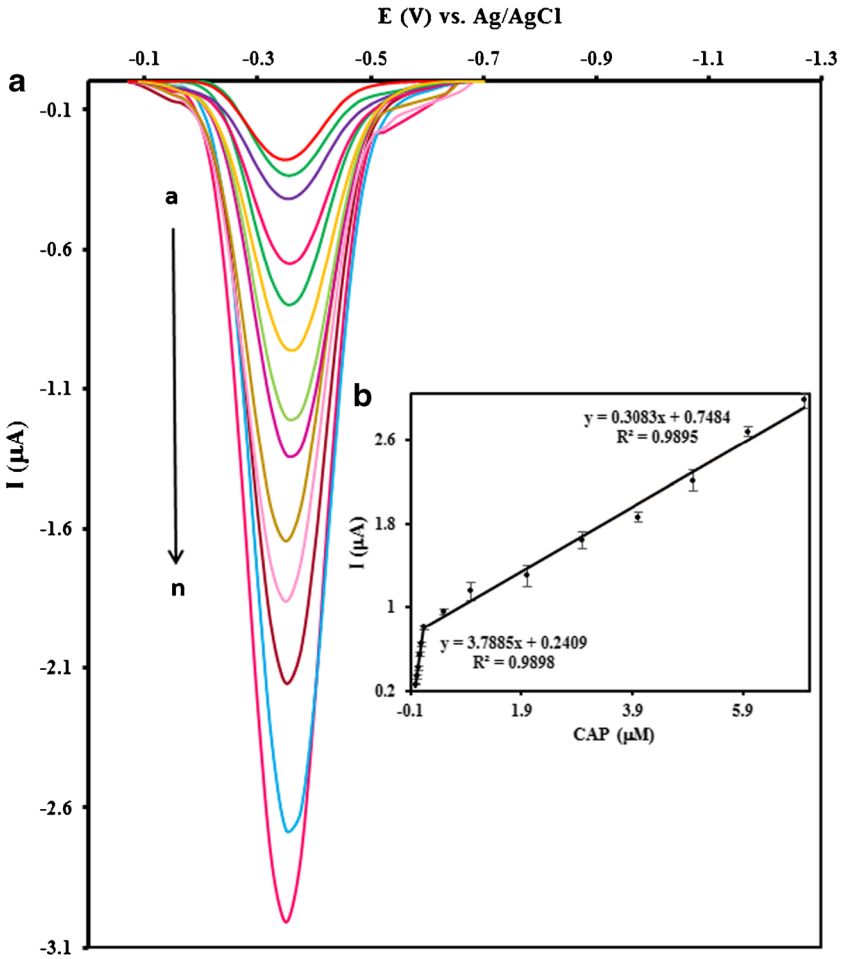

Fig. 4 (**A**) DPV signals of HEM/Apt/AuNPs/SBA-15@DABCO/SPE after incubation for 30 min with different CAP concentrations in the absence (a) and presence of different concentrations of CAP: (b) 0.03, (c) 0.05, (d) 0.075, (e) 0.1, (f) 0.15, (g) 0.5, (h) 1.0, (i) 2.0, (j) 3.0, (k) 4.0, (l) 5.0, (m) 6.0, and (n) 7.0 μM in 50 mM Tris–HCl buffer solution (pH 7.40). Inset **B** is the calibration plot of I_p vs. CAP concentration

aptamer, a reduction peak at −0.35 V in 50 mM TBS (pH 7.40) was observed which shows the capability of the HEM to bind to the aptamer (Fig. 3C, curve b). After incubation of the Apt/AuNPs/SBA-15@DABCO/SPE with 2.0 μM CAP, a further increase in the peak current for the HEM reduction was obtained in comparison with the curve b. This result demonstrated a successful identification of the CAP by the aptamer, which indicates that the HEM should be closer to the electrode surface (Fig. 3C, curve c).

Analytical characteristics of CAP aptasensor

Figure 4A shows the DPV responses of the different concentrations of CAP at the Apt/AuNPs/SBA-15@DABCO/SPE, in the presence of 20 μM HEM, in 50 mM TBS (pH 7.4). It was notable that peak currents increased with the increasing of the concentration of CAP. Figure 4B shows two linear response ranges of the constructed aptasensor from 0.03 to 0.15 μM and 0.15 to 7.0 μM based on analyzing the changes between the current of HEM reduction peak and the concentrations of CAP. The detection limit was calculated as 4 nM at 3σ. The reproducibility of the aptasensor was evaluated by using the following method. Eight HEM/Apt/AuNPs/SBA-15@DABCO/SPE electrodes were incubated with 2 μM CAP and all electrodes exhibited electrochemical responses with an average relative standard deviation (RSD %) of 1.20 %. Thus, the proposed aptasensor exhibited an acceptable stability for the detection of CAP.

Selectivity study

In order to determine the specificity of the aptamer for CAP, control experiments were performed using several drugs: 1.0 μM cefixime, 1.0 μM cephalexin, 1.0 μM amoxicillin, and 1.0 μM florfenicol (the results are shown in Fig. S2 in the ESM). The presence of even a 10-fold excess of non-target drugs caused a negligible current increase compared with that of the blank test. This result indicated that the binding event between the CAP and the aptamer is based on a selective recognition and thus the prepared biosensor is highly specific for CAP.

Application of aptasensor for detection of CAP in human serum

The applicability of the aptasensor was examined by measuring the CAP concentration in a blood serum sample using spike and recovery experiments. Recovery experiments were accomplished by adding the standard solutions of CAP with different concentrations to diluted human serum matrices. The analytical results shown in Table 1 indicate that the HEM/Apt/AuNPs/SBA-15@DABCO/SPE biosensor worked accurately for the analysis of CAP in the serum samples.

Table 1 Analysis of blood serum sample with CAP at different concentrations

Sample	Added (μM)	Detected (μM)	Recovery (%)	RSD (%)
1	3	2.8	93.3	0.8
2	0.9	0.83	92	1.2
3	0.1	0.09	90	1.9

Conclusion

In this study, a simple, rapid, and label-free aptasensor was created for detection of CAP by immobilizing the thiolated aptamer on the dendritic AuNPs/SBA-15@DABCO/SPE and using HEM as an effective electrochemical indicator. The immobilization of the AuNPs/SBA-15@DABCO on the SPE increased the surface area and conductibility of the aptasensor, which amplified the electrochemical signals. The interaction between the aptamer and CAP was investigated by CV, EIS, and DPV techniques. The reductive peak current of the HEM increased linearly with the addition of CAP in the concentration range of 0.03–0.15 μM and 0.15–7.0 μM with a detection limit as low as 4.0 nM. This biosensor showed a wide linear range, good sensitivity, and high selectivity for CAP and easily detects CAP in human serum samples.

Compliance with ethical standards

Conflict of interests The authors declare that there is no conflict of interests regarding the publication of this research result.

Healthy human serum sample for real sample analysis was supplied by the North Research Center, Pasteur Institute of Iran (Amol, Iran) with ethical approval.

References

1. Ellington AD, Szostak JW. In vitro selection of RNA molecules that bind specific ligands. Nature. 1990;346(6287):818–22.
2. Tuerk C, Gold L. Systematic evolution of ligands by exponential enrichment: RNA ligands to bacteriophage T4 DNA polymerase. Science. 1990;249(4968):505–10.
3. Clark SL, Remcho VT. Aptamers as analytical reagents. Electrophoresis. 2002;23(9):1335–40.
4. Kim D-K, Kerman K, Saito M, Sathuluri RR, Endo T, Yamamura S, et al. Label-free DNA biosensor based on localized surface plasmon resonance coupled with interferometry. Anal Chem. 2007;79(5):1855–64.
5. Minunni M, Tombelli S, Gullotto A, Luzi E, Mascini M. Development of biosensors with aptamers as bio-recognition

element: the case of HIV-1 Tat protein. Biosens Bioelectron. 2004;20(6):1149–56.
6. Patolsky F, Lichtenstein A, Willner I. Amplified microgravimetric quartz-crystal-microbalance assay of DNA using oligonucleotide-functionalized liposomes or biotinylated liposomes. J Am Chem Soc. 1999;122(2):418–9.
7. Chang H, Tang L, Wang Y, Jiang J, Li J. Graphene fluorescence resonance energy transfer aptasensor for the thrombin detection. Anal Chem. 2010;82(6):2341–6.
8. Zuo X, Song S, Zhang J, Pan D, Wang L, Fan C. A target-responsive electrochemical aptamer switch (TREAS) for reagentless detection of nanomolar ATP. J Am Chem Soc. 2007;129(5):1042–3.
9. Feng K, Sun C, Kang Y, Chen J, Jiang J-H, Shen G-L, et al. Label-free electrochemical detection of nanomolar adenosine based on target-induced aptamer displacement. Electrochem Commun. 2008;10(4):531–5.
10. Du Y, Li B, Wei H, Wang Y, Wang E. Multifunctional label-free electrochemical biosensor based on an integrated aptamer. Anal Chem. 2008;80(13):5110–7.
11. Wang X, Zhou J, Yun W, Xiao S, Chang Z, He P, et al. Detection of thrombin using electrogenerated chemiluminescence based on Ru(bpy)3(2+)-doped silica nanoparticle aptasensor via target protein-induced strand displacement. Anal Chim Acta. 2007;598(2):242–8.
12. Bruno JG, Kiel JL. Use of magnetic beads in selection and detection of biotoxin aptamers by electrochemiluminescence and enzymatic methods. Biotechniques. 2002;32(1):178–80. **182–173**.
13. Chandra P, Noh HB, Won MS, Shim YB. Detection of daunomycin using phosphatidylserine and aptamer co-immobilized on Au nanoparticles deposited conducting polymer. Biosens Bioelectron. 2011;26(11):4442–9.
14. Kashefi-Kheyrabadi L, Mehrgardi MA. Aptamer-conjugated silver nanoparticles for electrochemical detection of adenosine triphosphate. Biosens Bioelectron. 2012;37(1):94–8.
15. Martín-Aranda R, Čejka J. Recent advances in catalysis over mesoporous molecular sieves. Top Catal. 2010;53(3–4):141–53.
16. Barrosse-Antle LE, Bond AM, Compton RG, O'Mahony AM, Rogers EI, Silvester DS. Voltammetry in room temperature ionic liquids: comparisons and contrasts with conventional electrochemical solvents. Chem Asian J. 2010;5(2):202–30.
17. Walker AJ, Bruce NC, Walker AJ, Bruce NC. Cofactor-dependent enzyme catalysis in functionalized ionic solvents. Chem Commun. 2004;22:2570–1.
18. Fotouhi L, Shahrbanoo A, Omran M. Voltammetric response of furazolidone on multi-walled nanotube film coated carbon paste electrode using ionic liquid. Anal Bioanal Electrochem. 2013;5(3)283–90.
19. Lai Y, Ma Y, Sun L, Jia J, Weng J, Hu N, et al. A highly selective electrochemical biosensor for Hg2+ using hemin as a redox indicator. Electrochim Acta. 2011;56(9):3153–8.
20. Santos RM, Rodrigues MS, Laranjinha J, Barbosa RM. Biomimetic sensor based on hemin/carbon nanotubes/chitosan modified microelectrode for nitric oxide measurement in the brain. Biosens Bioelectron. 2013;44:152–9.
21. Chinnapen DJF, Sen D. Hemin-stimulated docking of cytochrome c to a hemin − DNA aptamer complex. Biochemistry. 2002;41(16):5202–12.
22. Alemu H, Hlalele L. Voltammetric determination of chloramphenicol at electrochemically pretreated glassy carbon electrode. Bull Chem Soc Ethiop. 2007;21(1):1–12.
23. Pilehvar S, Mehta J, Dardenne F, Robbens J, Blust R, De Wael K. Aptasensing of chloramphenicol in the presence of its analogues: reaching the maximum residue limit. Anal Chem. 2012;84(15):6753–8.
24. Viñas P, Balsalobre N, Hernández-Córdoba M. Determination of chloramphenicol residues in animal feeds by liquid chromatography with photo-diode array detection. Anal Chim Acta. 2006;558(1–2):11–5.
25. Wang A, Zhang L, Fang Y. Determination and separation of chloramphenicol and its hydrolysate in eye-drops by capillary zone electrophoresis with amperometric detection. Anal Chim Acta. 1999;394(2–3):309–16.
26. Rodziewicz L, Zawadzka I. Rapid determination of chloramphenicol residues in milk powder by liquid chromatography–electrospray ionization tandem mass spectrometry. Talanta. 2008;75(3):846–50.
27. Abjean JP. Planar chromatography for the multiclass, multiresidue screening of chloramphenicol, nitrofuran, and sulfonamide residues in pork and beef. J AOAC Int. 1997;80(4):737–40.
28. Li P, Qiu Y, Cai H, Kong Y, Tang Y, Wang D, et al. Simultaneous determination of chloramphenicol, thiamphenicol, and florfenicol residues in animal tissues by gas chromatography/mass spectrometry. Chin J Chromatogr. 2006;24(1):14–8.
29. Lindino CA, Bulhões LOS. Determination of chloramphenicol in tablets by electrogenerated chemiluminescence. J Braz Chem Soc. 2004;15:178–82.
30. Collado MS, Mantovani VE, Goicoechea HC, Olivieri AC. Simultaneous spectrophotometric-multivariate calibration determination of several components of ophthalmic solutions: phenylephrine, chloramphenicol, antipyrine, methylparaben and thimerosal. Talanta. 2000;52(5):909–20.
31. Bagheri Hashkavayi A, Bakhsh Raoof J, Ojani R, Hamidi Asl E. Label-free electrochemical aptasensor for determination of chloramphenicol based on gold nanocubes-modified screen-printed gold electrode. Electroanalysis. 2015;27(6):1449–56.
32. Laschi S, Palchetti I, Marrazza G, Mascini M. Development of disposable low density screen-printed electrode arrays for simultaneous electrochemical measurements of the hybridisation reaction. J Electroanal Chem. 2006;593(1–2):211–8.
33. Li H, Yang M, Pu Q. Palladium with spindle-like nitrogen ligand supported on mesoporous silica SBA-15: a tailored catalyst for homocoupling of alkynes and Suzuki coupling. Microporous Mesoporous Mater. 2012;148(1):166–73.
34. Baharfar R, Azimi R. Immobilization of 1,4-diazabicyclo[2.2.2]Octane (DABCO) over mesoporous silica SBA-15: an efficient approach for the synthesis of functionalized spirochromenes. Synth Commun. 2014;44(1):89–100.
35. Yuan C, Huang Z, Chen J. Basic ionic liquid supported on mesoporous SBA-15: an efficient heterogeneous catalyst for epoxidation of olefins with H2O2 as oxidant. Catal Commun. 2012;24:56–60.
36. Kalita P, Kumar R. Immobilization of 1,5,7-triazabicyclo[4.4.0]dec-5-ene over mesoporous materials: an efficient catalyst for Michael-addition reactions under solvent-free condition. Appl Catal A Gen. 2011;397(1):250–8.
37. Davarpanah J, Kiasat AR, Noorizadeh S, Ghahremani M. Nano magnetic double-charged diazoniabicyclo[2.2.2]octane dichloride silica hybrid: Synthesis, characterization, and application as an efficient and reusable organic–inorganic hybrid silica with ionic liquid framework for one-pot synthesis of pyran annulated heterocyclic compounds in water. J Mol Catal A Chem. 2013;376:78–89.
38. Li J-H, Hu X-C, Xie Y-X. Polymer-supported DABCO–palladium complex as a stable and reusable catalyst for room temperature Suzuki–Miyaura cross-couplings of aryl bromides. Tetrahedron Lett. 2006;47(52):9239–43.
39. Anand N, Ramudu P, Reddy KHP, Rao KSR, Jagadeesh B, Babu VSP, et al. Gold nanoparticles immobilized on lipoic acid functionalized SBA-15: synthesis, characterization and catalytic applications. Appl Catal A Gen. 2013;454:119–26.
40. Karimi B, Vafaeezadeh M. SBA-15-functionalized sulfonic acid confined acidic ionic liquid: a powerful and water-tolerant catalyst for solvent-free esterifications. Chem Commun. 2012;48(27):3327–9.